Mon. Not. R. Astron. Soc. **000**, 000–000 (0000) Printed 26 September 1997 (MN LaTeX style file v1.4)

The Surface Structure and Limb Darkening Profile of Betelgeuse.

D. Burns,[1] J. E. Baldwin,[1] R. C. Boysen,[1] C. A. Haniff,[1] P. R. Lawson,[1] C. D. Mackay,[2] J. Rogers,[1] T. R. Scott,[2] P. J. Warner,[1] D. M. A. Wilson[1] and J. S. Young[1]

[1] *Mullard Radio Astronomy Observatory, Cavendish Laboratory,Madingley Road, Cambridge, CB3 0HE, UK*
[2] *Institute of Astronomy, Madingley Road, Cambridge, CB3 0HA, UK*

Accepted 1997 Jun 27. Received 1997 Jun 19; in original form 1997 May 7

ABSTRACT

We present the first resolved image of a star observed with a separated-element optical aperture synthesis telescope. Observations of the M2 Iab supergiant Betelgeuse (α Orionis) were made at 830 nm with the Cambridge Optical Aperture Synthesis Telescope (COAST) during October 1995. Unusually, the source intensity distribution was highly symmetric at the time of observation – we find no evidence for the brightness asymmetries observed in earlier studies. Our data indicate a strongly limb-darkened but otherwise uniform and circularly symmetric disc, with no compact features contributing any more than 4 per-cent of the total flux from the source. The brightness profile is characterised by a very flat core and a Gaussian-like tail, and cannot be represented satisfactorily by a conventional low-order Taylor expansion. A two-parameter Gauss-Hermite polynomial expansion provides a good description for the centre-to-limb brightness distribution.

Key words: techniques: interferometric – telescopes – stars: imaging – stars: supergiants – stars: individual: Betelgeuse – stars: atmospheres.

1 INTRODUCTION

The prominence of α Orionis as the largest and brightest nearby cool supergiant has made it the preferred target for many high angular resolution imaging studies. The principal results of these have been numerous angular diameter estimates, and, more recently, the detection of surface and circumstellar structures. The angular sizes derived for the star have been reasonably consistent, lying in the range 50 ± 10 milliarcseconds (mas), and show evidence for a certain amount of wavelength dependence. This encompasses both a slow decrease in angular size with wavelength together with anomalously large sizes seen in the TiO absorption bands (see, e.g. Cheng et al. (1986) for a review). At mid-infrared wavelengths emission from warm circumstellar dust has been observed (Danchi et al. 1994), most recently very close to the stellar photosphere (Bester et al. 1996).

Small-scale asymmetries in the emission from the star were first detected unambiguously using aperture synthesis methods by Buscher et al. (1990), and have subsequently been confirmed by further interferometric studies at optical wavelengths (Wilson et al. 1992; Tuthill, Haniff & Baldwin 1997), and by UV imaging with the HST (Gilliland & Dupree 1996). These features appear as unresolved bright spots superposed on the stellar disc and can contribute as much as 15% of the total emission from the star. In most instances one or two spots have been seen but some data show evidence for at least three separate features. The changes in the position and brightness of the features occur on time-scales as short as one month and images taken several months apart sometimes show no obvious relationship to one another (Tuthill et al. 1997; Wilson et al. 1997).

The main shortcoming of these previous optical/UV studies has been a lack of spatial resolution — typical large telescopes can only probe structures larger than ~ 25 mas at visible wavelengths. Improvements in angular resolution, via the interferometric combination of arrays of telescopes, thus offer the possibility of investigating a number of outstanding issues including the sizes and shapes of the brightness asymmetries and the detailed form of the star's limb-darkening curve.

In this paper we present the first observations of Betelgeuse obtained with the Cambridge Optical Aperture Synthesis Telescope (COAST). These have allowed exploration of the visibility function of the star beyond its first null, and place new constraints on the angular diameter, the surface structure, and the centre-to-limb intensity profile of the star. Furthermore, they provide the first demonstration of the feasibility of imaging a resolved stellar disc using an optical synthesis array.

© 0000 RAS

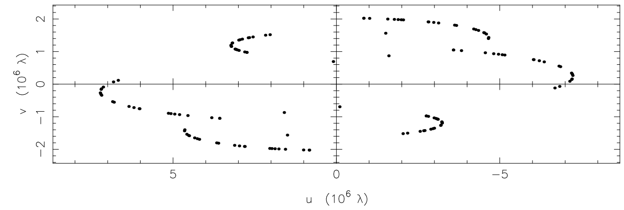

Figure 1. Fourier plane coverage for the observations reported here. Due to the extreme projection of some of the interferometer baselines the synthesised beam is highly elliptical with a central core of FWHM 17 mas $\times$ 54 mas in position angle 8.9°. The longest projected baseline has a length of 6.0 m (7.2Mλ).

Table 1. Observation log. The dates refer to the start of the night of each observation and N_{vis} and N_{cl} to the number of visibility and closure-phase measurements made. An identical number were made for the calibration source. Each "measurement" corresponds to 99 seconds of observations. τ_c is the coherence time at 830 nm, i.e. the length of time over which the autocorrelation-function of an APD output fell to half its zero-delay value: this characterises the longest useful coherent integration time.

Date	$\lambda/\Delta\lambda$ (nm)	N_{vis}	N_{cl}	Calibrator star	τ_c	Total observing time (s)
95/10/20	830/40	47	12	γ Ori	7.3	11682
95/10/23	830/40	29	16	γ Ori	2.7	8910
95/10/29	830/40	30	13	γ Ori	10.8	8514
95/10/31	830/40	3	1	γ Ori	4.4	792

2 OBSERVATIONS AND DATA REDUCTION

2.1 COAST

COAST is an earth-rotation optical/IR synthesis array of 4 telescopes, each of which can be moved between a number of fixed stations so as to provide interferometer baselines between 2 and 100 m. Because more than 2 array elements are available, COAST differs from earlier optical interferometers in being able to measure the closure-phases that are required for successful interferometric imaging. Each element of COAST comprises a 0.5 m siderostat feeding a horizontal 0.4 m Cassegrain telescope. The light from each telescope is fed back via fast-guiding mirrors into a central laboratory where all the beams are combined using an arrangement of beam-splitter plates. Other components within the building allow equalisation of the light paths of the beams (using delay-lines employing a system of roof mirrors mounted on motorised servo-controlled trolleys), real-time stabilisation of the beam directions, and detection of the fringes using photon-counting silicon avalanche photo-diodes (APDs).

The interference fringes between every pair of combined beams are realized at the detectors by scanning each of the delay lines with a linear sweep of amplitude $\sim 30\mu$m, i.e. somewhat larger than the coherence length of the light transmitted by the narrow-band filters in front of the APDs. By using appropriately chosen amplitudes, or speeds, for all 4 delay-line trolleys, the 6 possible interference fringes can be separated in the output of each APD as different temporal frequencies.

2.2 Observations

Measurements of Betelgeuse were obtained on 4 nights over a period of 11 days in 1995 October when only three elements of the array were operational, giving a maximum baseline of 6.1 m. Over this period Betelgeuse faded at visual wavelengths by several hundredths of a magnitude (Krisciunas & Luedeke 1996). While easily observable, this is a small enough fraction of its typical variation (several tenths of a magnitude) that we expect any resulting changes in its visual appearance to have been small. In order to sample short as well long baselines, observations were secured over as wide a range of Hour Angle as possible (see Fig. 1), some with the source at elevations less than 25°. The combined beams were stopped down to a 16 cm effective diameter within the optics laboratory to match the local seeing conditions of $\sim 1.5''$, and an observing wavelength of 830 nm was selected using 40 nm-wide (FWHM) interference filters.

Each observation of Betelgeuse was interleaved with a similar observation of an unresolved calibration star so as to measure the instrumental and atmospheric coherence losses, and to estimate the level of systematic errors in the experiment. For the observations reported here the B2 giant, γ Orionis, was employed, its proximity to Betelgeuse outweighing the large difference in spectral type and magnitude between the two stars.

Measurements of the source visibility function were performed on each baseline sequentially by allowing only two of the input beams into the optics laboratory at any one time. Under these circumstances each of the 4 APDs provided simultaneous and independent data-streams from which to estimate the visibility amplitudes. Closure-phase data were secured by combining light from all 3 operational telescopes simultaneously. Again, each APD provided an independent data-stream from which estimates of the 3 visibility amplitudes and 1 closure-phase were derived. In all cases data streams of 99 seconds were recorded. Full details of the observations, including the dates and total number of measurements are given in Table 1.

2.3 Data Reduction

2.3.1 *Visibility Amplitudes*

Estimates of the source visibility amplitudes were made by Fourier transformation of segments of data corresponding to single sweeps of the fringe envelope past a given APD. The power spectra from the 990 such sweeps obtained in any 99 second observation were summed to give an averaged spectrum with high signal-to-noise. Examples of these mean spectra for low and high-visibility fringes are shown in Fig. 2. Estimates of the uncalibrated fringe power were then obtained by integrating underneath the signal peak above a low-level background due to photon statistics and atmospheric effects. The integrated spectral power was then divided by the square of the mean photon rate and the square root taken, to give an estimate of the uncalibrated root mean square visibility amplitude $\sqrt{\langle V^2 \rangle}$. This value was normalised by a similarly calculated quantity for the calibrator source to give the adopted value of the visibility amplitude.

All four APD outputs were analysed in this manner and the average of the 4 independent results adopted as the "best

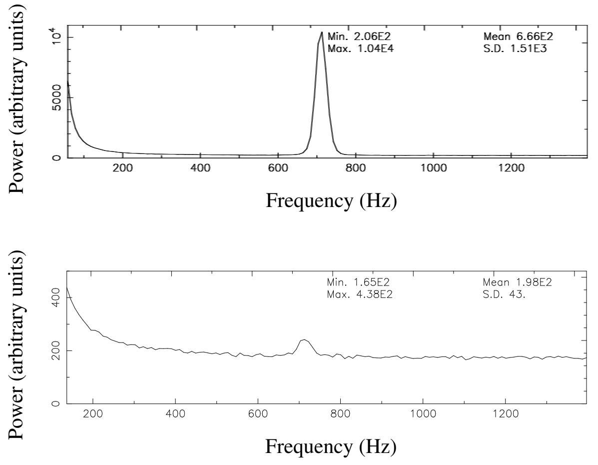

Figure 2. Mean power spectra, averaged over a 99 s observation of high- (17.5%, top) and low- (0.9%, bottom) visibility fringes. Three main features can be seen: first, a peak at 715 Hz corresponding to the mean scan rate of the fringes past the detector, second, a DC peak broadened by atmospheric scintillation and often extending up to 200 Hz, and, third, a negatively sloping background.

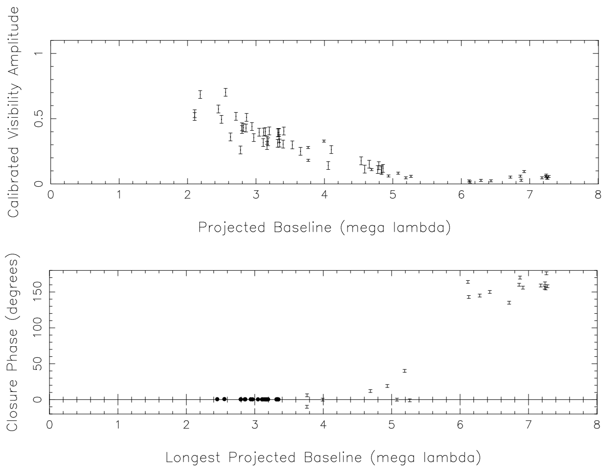

Figure 3. Calibrated visibility amplitudes (top) and closure-phases (bottom) for Betelgeuse plotted as functions of projected baseline length in wavelengths. The scatter of the measured amplitudes above visibilities of ~ 0.5 reflects the low source altitudes (and hence poorer and less stable seeing) at which Betelgeuse had to be observed to secure data on short baselines. For the closure-phases the projected length of the longest baseline has been used as the abscissa. Note that the value of the closure-phase flips from 0° to $\sim 180^\circ$ as the visibility amplitude reaches zero, indicating the crossing of a visibility null for a symmetric source.

estimate" for the visibility amplitude of the source. After most of the systematic effects had been removed by calibration, the formal residual errors in the visibility amplitudes were typically in the range 3 to 10 per-cent of the visibility.

2.3.2 *Closure-Phases*

To derive closure-phases, segments of the data streams containing fringes from all three baselines were integrated coherently with appropriate sine and cosine weighting functions in order to form estimates of the complex visibility unique to each baseline. To preserve the information content of the data, the integrations were performed over a short timescale, τ_c, equal to the time over which the autocorrelation function of a stream of data containing fringes fell by a factor of 2. The triple products of these "instantaneous" visibilities were formed for each coherent segment, and this quantity averaged over all the data segments. The argument of the mean triple-product was then adopted as the value of the closure-phase.

The errors in the derived closure-phases were typically 2°. Unresolved sources, for which the closure-phases were expected to be 0°, gave values of $0^\circ \pm 2^\circ$ suggesting that there was a low degree of cross-talk between the three baselines and only small residual systematic errors.

3 RESULTS

3.1 Fourier Measurements

The calibrated visibility amplitudes and closure-phases recovered for Betelgeuse are presented in Fig. 3. Three main features are immediately apparent:

(i) the visibility function falls with baseline, reaching a minimum of $\simeq 1$ per-cent between 5Mλ and 6Mλ, and then rises again.
(ii) the values of the closure-phases are either $\sim 0^\circ$ or $\sim 180^\circ$, and depend only on the length of the longest projected baseline.
(iii) the transition from 0° to 180° in the closure-phase corresponds to a minimum of the visibility amplitude.

While many previous investigations of Betelgeuse have provided visibility amplitude and closure-phase data (see, e.g. Buscher et al. 1990), the results presented here are highly unusual. Most importantly, the independence of the closure-phase on the orientation of the interferometer baselines is strong evidence for a high degree of symmetry in the source brightness distribution at the time of the observations. Furthermore, the transition in closure-phase value from $\sim 0^\circ$ to $\sim 180^\circ$ as the visibility amplitude approaches zero is indicative of measurements being made beyond the first null in the transform of a symmetric disc. There thus appear to be no signatures of any asymmetric structure on the star.

3.2 Source Structure

To confirm the above interpretation, the visibility amplitudes and closure-phases from October 20th and 29th were mapped using a standard implementation of self-calibration within the Caltech VLBI package (Pearson 1991). The resulting image is shown in Fig. 4. Note that because of the non-uniform Fourier-plane coverage of the dataset the reconstructed image shares the elongation of the synthesised beam, which is an ellipse with FWHM of 17 mas $\times$ 54 mas in position angle 8.9°.

Apart from this imprint of the Fourier-plane coverage,

© 0000 RAS, MNRAS **000**, 000–000

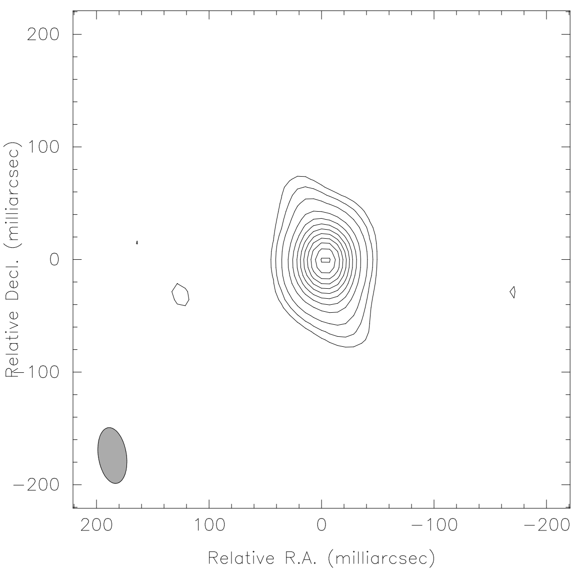

Figure 4. Self-calibration image of Betelgeuse at 830 nm obtained from data of 1995 October 20th and 1995 October 29th. Contours are plotted at 2.5, 5, 10, 20, 30, 40, 50, 60, 70, 80, 90 & 99 per-cent of the peak flux. The beam is illustrated in the bottom left hand corner. The RMS background flux is of the order of 1 per-cent of the peak flux and therefore mainly invisible in this image. North is to the top and East to the left.

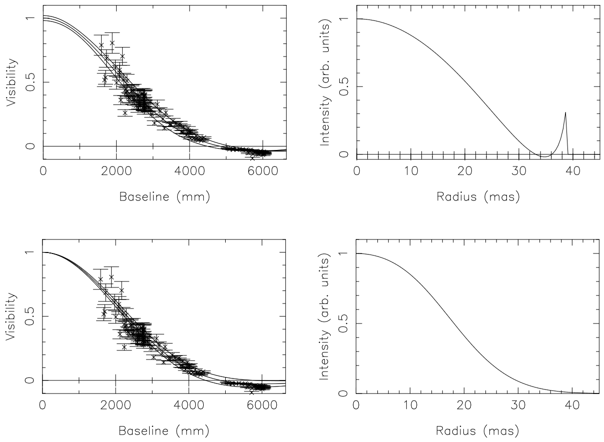

Figure 5. Model-fits between the measured Fourier data and Taylor (top-left) and Gauss-Hermite (bottom-left) models. The central curves represent the visibility functions with the maximum posterior probability while the others delineate the $\pm 3\sigma$ errors. For each model the right-hand panel shows the intensity distribution corresponding to the best-fit model. Note that, for the Taylor expansion, the intensity distribution near the edge of the star first goes negative then rises sharply, indicating that this type of model is poorly suited to the analysis of strongly limb-darkened discs.

the map shows no evidence for anything other than a symmetric disc — no asymmetric surface structures reported on earlier occasions in the literature are present. Furthermore, there are only two weak noise peaks visible (at a level of 3 percent of the peak flux) in the half arcsecond field-of-view. The dynamic range of the map, i.e. the ratio of the peak flux in the map to the rms noise away from the map centre, is thus of order 100:1. This can be compared with the value expected on the basis of the number and quality of the individual Fourier measurements used to make the map, i.e.

$$\langle \sigma_I / I \rangle \sim \langle \sigma_v / v \rangle / \sqrt{N_v},$$

where σ_I is the noise in the map intensity I, N_v is the total number of visibilities used, and $\langle \sigma_v / v \rangle$ is the mean fractional error in each visibility datum. For Fig. 4, $N_v = 69$ and $\langle \sigma_v / v \rangle \simeq 0.05$, which gives a value of σ_I / I of 0.006, in good agreement with the value of 0.01 measured from the map itself.

Rather than attempting to quantify the apparent symmetry of Betelgeuse directly from our image, the calibrated Fourier data were used as constraints in two model-fitting procedures. In the first of these, a point source was added to the CLEAN-component model arising from the self-calibration mapping. The position and flux of this additional component were then adjusted so as to delimit the allowed range of parameter space in which a good least-squares fit between the model and data could be obtained. A second, Bayesian, analysis was also performed, in which the posterior probabilities of different models (comprising numbers of delta-functions superposed on an otherwise uniform elliptical disc) were evaluated and compared.

Both methods gave comparable results, and imply that a maximum of 4 per-cent of the total source flux was present in any unresolved feature, the remainder being disposed in a circularly symmetric fashion. If present, the most probable location for any compact component was between 5 and 20 mas from the centre of the star along PA $-80°$. However, the relatively poor constraint on the position vector, and its alignment with the direction of maximum resolution would also be consistent with the presence of a limb-darkened disc. It seems likely then that our estimate for the maximum "spot" flux of 4 per-cent is a hard upper limit.

This lack of asymmetry is certainly unusual for Betelgeuse. Recent studies, whether by interferometry (see, e.g. Tuthill et al. 1997; Wilson et al. 1997) or conventional imaging (Gilliland & Dupree 1996), have consistently revealed the presence of compact unresolved structures contributing many tens of per-cent of the emission from the star. These "hotspots" are known to evolve on monthly timescales, but as yet their origin has not been uniquely identified. The most favoured models invoke either giant convection cells (Stothers & Leung 1971; Stothers 1972) or supergranulation (Schwarzchild 1975). Neither of these models are ruled out by our new observations.

Although our data were obtained at a slightly longer wavelength than earlier interferometric studies, if the hotspots are caused by moderate (e.g. a few hundred Kelvin) temperature excesses on an otherwise uniform 3500 K stellar disc then a change in observing wavelength from 700 nm (a wavelength often used for interferometric observations of Betelgeuse) to 830 nm would not be expected to have had a significant effect on the apparent contrast of any features. Similarly, it is unlikely that the inner dust shell formed in 1994 (Bester et al. 1996) can have masked any underlying surface features since its optical depth at visual wavelengths is predicted to have been small. The fact that Betelgeuse was unusually bright at the time of our observations (Krisciunas & Luedeke 1996) may, however, have had a bearing on its apparent morphology, perhaps by spatial averaging of numerous convective plumes, but any further elaboration on this point will clearly require a more substantial database.

3.3 Limb-darkening

Given the lack of asymmetric structure on Betelgeuse at the time of our observations, and the availability of Fourier measurements beyond the first null in the visibility function, we have used our data to investigate both the diameter and limb-darkening profile of the star.

For these analyses we have assumed that there was no contribution from any large scale structure arising from the thin inner dust shell (radius $\sim 0.1''$) detected by Bester et al. (1996). While the measurements of Wilson et al. (1997) from late 1994 show evidence for a large scattering halo at 700 nm contributing approximately 15 per-cent of the emission from the star, mid-infrared spectra taken during 1995 show the strength of the 9.7 μm silicate feature falling (Bester et al. 1996), and so any scattering halo present in 1995 October is likely to have contributed a smaller fraction (< 10 per-cent) of the total emission. The corrections associated with the presence of such a feature are, however, very small, and lead to downward revisions of approximately 1-sigma to the scale parameters reported below.

To permit comparison with similar datasets in the literature, we initially used only those measurements on baselines less than 4 m to estimate the stellar diameter. Fits of circularly symmetric uniform discs and Gaussian functions gave diameters of 51.1 ± 1.5 mas and 35.1 ± 1.5 mas (FWHM), in good agreement with the corresponding estimates of Mozurkewich et al. (1991), who measured a uniform-disc diameter of 49.4 ± 0.24 mas at 800 nm, and Christou, Hebden & Hege (1988), who give a Gaussian FWHM of 30.6 mas at 850 nm.

Bayesian analyses of all of the Fourier data were subsequently made using two distinct, and more complex, models for the stellar brightness profile. The first of these employed a conventional Taylor expansion in μ (the cosine of the angle between the line of sight to the observer and the normal to the surface of the star: $\mu^2(r) = 1 - r^2/r_o^2$), such that

$$\frac{I(r)}{I_0} = \begin{cases} 1 - \sum_{n=1}^{n_{max}} \alpha_n \Big(1 - \mu(r)\Big)^n & \text{if } r < r_o \\ 0 & \text{if } r > r_o \quad , \end{cases}$$

where $\{\alpha_n\}$ are the limb-darkening coefficients, r_o is the stellar radius, and n_{max} is the order of the expansion. The posterior probability of these models was maximised for a second order expansion, within which the most favoured parameter values were $r_o = 39.15 \pm 1.76$ mas, $\alpha_1 = 3.75 \pm 0.03$, and $\alpha_2 = -3.45 \pm 0.05$. However, while the fit of this model to the data was satisfactory (see Fig. 5), the corresponding brightness distribution showed clear unphysical behaviour towards the edge of the stellar disc. This reflects the inadequacy of such models to correctly reproduce the heavily limb-darkened profiles of stars such as Betelgeuse without admitting extremely high order expansions.

In an effort to overcome this problem, a second type of model, involving a Gauss-Hermite expansion, was developed in which the stellar brightness profile was modelled as:

$$\frac{I(r)}{I_o} = \left(1 + \sum_{n=1}^{n_{max}} \alpha_n H_{2n}(r/r_o)\right) \exp(-r^2/2r_o^2) \, .$$

Here the H_{2n} are the Hermite polynomials of even order, $\{\alpha_n\}$ are a new set of expansion coefficients, and r_o is the stellar scale parameter. Full details of this model, and its rationale, can be found in Burns (1997). For this type of model, the posterior probability was maximised for a first order expansion, where the optimal parameter values were $r_o = 25.23 \pm 0.57$ mas and $\alpha_1 = 0.085 \pm 0.005$. The agreement between this model and the visibility measurements, together with the corresponding stellar intensity profile, are shown in the bottom two panels of Fig. 5.

Despite being characterised by one fewer free parameter, the posterior probability is higher for the Gauss-Hermite expansion, and it is able to give an excellent fit to the visibility data without introducing any unphysical behaviour in the intensity at large radii. The results of our analysis suggest that during 1995 October the surface brightness distribution of Betelgeuse was highly limb-darkened with essentially no emission present at radii in excess of 40 mas.

Although Betelgeuse has been observed using high angular resolution techniques many times before, few of these earlier studies have successfully explored the centre-to-limb brightness profile of the star. Given the unusual nature of this profile we feel that it is makes little sense to quote a limb-darkening corrected value for the stellar diameter without reference to a specific form for the brightness distribution. However, the analysis presented here represents an important first in providing a realistic constraint on the properties of theoretical models of the structure of cool stellar atmospheres.

4 SUMMARY

We have presented new interferometric observations of the M supergiant Betelgeuse obtained with COAST. These have been used to construct the first optical synthesis image of a resolved source obtained with a separated-element interferometer. The resulting spatial resolution and image quality are in good agreement with theoretical expectations and suggest that imaging of complex sources with similar arrays will be relatively straightforward. At the time of the observations, in 1995 October, the brightness distribution of the star showed none of the asymmetric structure that has featured in previous investigations. Rather, our data imply the presence of a circularly symmetric disc, with an unusual flat-topped and strongly limb-darkened profile that cannot conveniently be represented by a conventional Taylor expansion in μ. A two-parameter Gauss-Hermite expansion provides a good description of the brightness profile.

ACKNOWLEDGMENTS

The authors are grateful to the numerous technical and support staff at Lord's Bridge Observatory without whose assistance the construction and operation of COAST would have been impossible. CAH is grateful to The Royal Society and TRS to the C. T. Taylor fund for financial support. The construction of COAST has been supported by SERC, PPARC and the University of Cambridge.

REFERENCES

Burns D., 1997, MNRAS, In preparation
Bester M., Danchi W.C., Hale D., Townes C.H., Degiacomi C.G., Mekarnia D., Geballe T.R., 1996, ApJ, 463, 336
Buscher D.F., Haniff C.A., Baldwin J.E., Warner P.J., 1990, MNRAS, 245, 7p
Cheng A.Y.S., Hege E.K., Hubbard E.N., Goldberg L., Strittmatter P.A., Cocke W.J., 1986, ApJ, 309, 737
Christou J.C., Hebden J.C., & Hege E.K., 1988 ApJ, 327, 894
Danchi W.C., Bester M., Degiacomi C.G., Greenhill L.J., Townes C.H., 1994, AJ, 107, 1469
Gilliland R.L., Dupree A.K., 1996, ApJ, 463, L29
Krisciunas K., & Luedeke K.D., Information Bulletin On Variable Stars (4355), Comissions 27 and 42 of the IAU. (1996)
Mozurkewich D., Johnston K.J., Simon R.S., Bowers P.F., Gaume R., Hutter D.J., Colavita M.M., Shao M., & Pan X.P., 1991, Astron. J. 101, 2207
Pearson T.J., 1991, BAAS, 23, 991
Schwarzchild M., 1975, ApJ, 195, 137
Stothers R., 1972, Astron. Astrophys., 18, 325
Stothers R., & Leung K.C., 1971, Astron. Astrophys., 10, 290
Tuthill P.G, Haniff C.A., Baldwin J.E., 1997, MNRAS, 285, 529
Wilson R.W., Baldwin J.E., Buscher D.F., Warner P.J., 1992, MNRAS, 257, 369
Wilson R.W., Dhillon V.S., Haniff C.A., 1997, MNRAS, In press.

This paper has been produced using the Blackwell Scientific publications LATEXstyle file.